Second harmonic generation imaging microscopy studies of *osteogenesis imperfecta*

Oleg Nadiarnykh
University of Connecticut Health Center
Department of Cell Biology
Center for Cellular Analysis and Modeling
Farmington, Connecticut 06030

Sergey Plotnikov
Laboratory of Cell and Tissue Morphodynamics
National Heart, Lung, and Blood Institute
National Institutes of Health
Bethesda, Maryland 20892

William A. Mohler
University of Connecticut Health Center
Department of Genetics and Developmental Biology
Center for Cellular Analysis and Modeling
Farmington, Connecticut 06030

Ivo Kalajzic
University of Connecticut Health Center
Department of Reconstructive Services
Farmington, Connecticut 06030

Deborah Redford-Badwal
University of Connecticut Health Center
Department of Oral Rehabilitation
Department of Craniofacial Sciences
Farmington, Connecticut 06030

Paul J. Campagnola
University of Connecticut Health Center
Department of Cell Biology
Center for Cellular Analysis and Modeling
Farmington, Connecticut 06030

Abstract. We have used quantitative second harmonic generation (SHG) imaging microscopy to investigate the collagen matrix organization in the oim mouse model for human *osteogenesis imperfecta* (OI). OI is a heritable disease in which the type I collagen fibrils are either abnormally organized or small, resulting in a clinical presentation of recurrent bone fractures and other pathologies related to collagen-comprised tissues. Exploiting the exquisite sensitivity of SHG to supramolecular assembly, we investigated whether this approach can be utilized to differentiate normal and oim tissues. By comparing SHG intensity, fibrillar morphology, polarization anisotropy, and signal directionality, we show that statistically different results are obtained for the wild type (WT) and disease states in bone, tendon, and skin. All these optical signatures are consistent with the collagen matrix in the oim tissues being more disordered, and these results are further consistent with the known weaker mechanical properties of the oim mouse. While the current work shows the ability of SHG to differentiate normal and diseased states in a mouse model, we suggest that our results provide a framework for using SHG as a clinical diagnostic tool for human OI. We further suggest that the SHG metrics described could be applied to other connective tissue disorders that are characterized by abnormal collagen assembly. [DOI: 10.1117/1.2799538]

Keywords: second harmonic generation; nonlinear optics; tissues, lasers in medicine; microscopy; scattering.

Paper 07054SSR received Feb. 15, 2007; revised manuscript received Jul. 6, 2007; accepted for publication Aug. 9, 2007; published online Oct. 29, 2007.

1 Introduction

While significant technological advances have greatly improved the capabilities of ultrasound, magnetic resonance, computed tomography, and positron emission tomography imaging, these modalities are practically limited to resolutions of ~1 mm. However, much higher spatial resolution (1μm or less) is required to visualize structural changes associated with diseased cells and tissues. Historically, analysis at this anatomical level has been achieved by histology, which involves the removal of tissue, fixing and slicing into thin sections, and staining with contrast-increasing dyes. While histology remains the "gold standard" for pathologists, this approach is inherently highly subjective, as the accuracy depends on the experience and skill of the interpreting clinician. There remains a clear need for quantitative optical microscopy approaches that can be performed either *in vivo* or *ex vivo* on intact tissues, thus eliminating the artifacts and other pitfalls inherent in the interpretation of histological sections.

To address this issue, we have been investigating whether second harmonic generation (SHG) imaging microscopy can differentiate normal and abnormal tissue structure. Over the last several years, SHG has emerged as a powerful new biological and biophysical imaging modality, where it has been demonstrated that structural protein arrays consisting of collagen,[1–4] acto-myosin,[1,5,6] and tubulin[1,7] exhibit large hyperpolarizabilities that produce bright SHG contrast. Perhaps the primary benefit afforded by this method is the direct visualization of the supramolecular assembly without any exogenous contrast increasing agents. Furthermore, we have previously shown that the method provides more structural information than possible through the use of fluorescent

Address all correspondence to Paul J. Campagnola, University of Connecticut Health Center, Department of Cell Biology, Center for Cellular Analysis and Modeling, MC-1507, 263 Farmington Avenue, Farmington, CT 06030; Tel: 860–679–4354; Fax: 860–679–1039; E-mail: campagno@neuron.uchc.edu

1083-3668/2007/12(5)/051805/9/$25.00 © 2007 SPIE

labels.[1] This is because SHG is a second-order nonlinear optical process and requires a noncentrosymmetric environment to produce contrast. This constraint makes SHG an exquisitely sensitive probe of the alignment in tissues and may lead to great potential as a clinical diagnostic tool. For example, many connective tissue diseases including osteoporosis and osteoarthritis are characterized by abnormal collagen assembly, and SHG may reveal differences in the morphology of diseased fibers not possible by other optical methods. In addition to being dependent on the molecular assembly, the SHG contrast is also reflected in the concentration of "harmonophores." This also has relevance as a disease diagnostic, as several disorders including *osteogenesis imperfecta* (OI) and scleroderma are characterized by insufficient and excessive concentrations of collagen, respectively. SHG has also shown early promise in imaging cancerous tissues, since malignant tumors often have increased levels of collagen relative to normal tissue. For example, using a mouse model, Brown and co-workers exploited this property and demonstrated that SHG was indeed sensitive to these concentration differences.[8] Similarly, Lin and co-workers showed abnormal collagen assembly (based on reduced SHG intensity) in basal cell carcinoma lesions.[9] Thus, SHG appears well-poised to make the successful transition from "bench to bedside."

In this paper we show how SHG imaging can be used to differentiate normal and OI diseased tissues. OI is a heritable disease of humans characterized by recurrent bone fractures, stunted growth, defective teeth, and other symptoms from abnormal tissues comprised of type I collagen. Because of its dramatic clinical presentation, OI has been at the leading edge of discovery of the methodologies and principles that apply for all heritable diseases of connective tissue. OI results from mutations within the Col1A1 or Col1A2 genes that affect the primary structure of the collagen chain and that induce changes in the secondary structure of the collagen trimers that incorporate the mutant chains. The ultimate outcome is collagen fibrils that are either abnormally organized, small, or both. The consequences are most dramatic in bone in which the weakened matrix stimulates the osteoclasts to remove the defective matrix. Although osteoblasts synthesize a new matrix, the new structure is no better than the original, and as a result, a never-ending spiral of bone resorption and new bone formation is established. The high bone turnover state precludes the accumulation of sufficient matrix to prevent recurrent bone fractures. It is generally assumed that the severity of the disease is related to the disruptive effect of the mutation on collagen fiber formation. For example, more disruptive mutations result in less (and less ordered) collagen secreted from the cell, resulting in more unstable fibers within the extracellular matrix. However, the ability to predict what type of mutation will have a mild or severe phenotype has not been perfectly successful. There remains a need to improve the phenotype/genotype connection.

As a first step toward solving this problem, we use SHG imaging to perform quantitative comparisons between normal and OI tissues using the oim murine model, which has the same phenotype (albeit different genotype) as human type III OI.[10] In these endeavors, we use several SHG metrics based on image intensity, tissue morphology, polarization analysis, signal directionality, and concurrent photon propagation properties. We initially demonstrate that SHG reveals profound morphological differences between wild type (WT) and oim bone. Although we note a high sensitivity of the fibrillar organization in bone to oim mutations, bone has a complex structure, and the resulting SHG images are difficult to quantify. While the primary OI clinical presentation is in bone, the defect is expressed in other type I collagen-containing tissues including tendon and skin. We therefore exploit the regularity of the fibrils in tendon to perform our initial quantitative analyses and establish quantitative metrics to distinguish the normal and disease states. Last, as we ultimately seek to apply this methodology to true *in vivo* clinical applications, we need to establish that SHG imaging of skin can be used as a diagnostic approach for OI. This is because skin is the most assessable tissue for either *in vivo* or *ex vivo* imaging. We show that the collective outcomes of these measurements are indicative of a more disorganized collagen structure, consistent with the observed phenotype of a weaker matrix and persistent bone fractures.

2 Experimental Methods

2.1 *Microscope and Imaging*

The SHG imaging system consists of a laser scanning head (Olympus Fluoview 300) mounted on an upright microscope (Olympus BX61), coupled to a mode-locked Titanium Sapphire laser. All measurements were performed with a laser fundamental wavelength of 900 nm with average power of 5 to 50 mW at the specimen. The system is designed for simultaneous SHG detection of the forward and backward components. In the former, a long working distance 40×0.8 N.A. water-immersion objective and a 0.9 N.A. condenser provide excitation and signal collection, respectively. The backward component is collected through the objective in a nondescanned configuration. In both geometries, the SHG signal is isolated with a longwave pass dichroic mirror and 10-nm bandpass filters (450 nm). The signals are detected by a pair of identical photon-counting photomultiplier modules (Hamamatsu). The SHG wavelength (450 nm) was confirmed with a fiber optic spectrometer (Ocean Optics). There is no detectable autofluorescence for collagen at this excitation wavelength.

Three-dimensional (3-D) SHG image stacks were quantitatively analyzed with ImageJ software (http://rsb.info.nih.gov/ij/). A coumarin dye slide emitting two-photon excited fluorescence at the SHG wavelength was used to calibrate both signal collection channels to account for uneven losses in optical paths and relative collection efficiency of the two detectors. Since the forward-to-backward fluorescence ratio from a dye slide is assumed to be one, it becomes the normalization factor for the two channels.

The input polarization is controlled by a set of half- and quarter-wave plates. We determined *de facto* the polarization of excitation light at the focal plane by matching SHG maxima and minima to those previously measured for linear (myofibrils) and spherical (dye-labeled spherical cells) specimens. For measurements not involving polarization analysis, circular polarization of the laser fundamental was used for the excitation. We adapted both acquisition channels for analysis of the polarization of the emitted SHG signals by addition of collimation lenses and Glan laser polarizers. Images were taken with the analyzing polarizers in the parallel and or-

thogonal positions to the excitation light to calculate the resulting anisotropy.

2.2 *Tissue Preparation*

Mice carrying the oim mutation are maintained in the B6C3Fe-a/a(C57BL/6JLe X C3HeB/FeJLe) hybrid background.[10] These mice were additionally crossbred with a pOBCol3.6GFP transgenic aCD-1 outbred strain in our facility. The oim/oim mice can be distinguished from the WT by their body phenotype (smaller size and weight and presence of limb deformities due to fractures). The genotype was confirmed by a previously described PCR analysis.[11] Imaging measurements were made within 3 h of sample excision. The overall thicknesses of the biopsies were $\sim 100\ \mu$m and contained the epidermis, dermis, and adipose layers.

Femurs from 3-month-old oim/oim and WT mice were fixed in 4% paraformaldehyde for 3 days followed by decalcification in 15% EDTA for 3 to 4 days. The bones were then soaked in 30% sucrose in PBS for 1 day. All the processes of fixation, decalcification, and cryoprotection were done at $4\,^{\circ}$C under constant agitation. Samples were embedded in frozen embedding medium (Thermo Shandon) at $-70\,^{\circ}$C, and 5-μm-thick full-length sections were made with the assistance of the CryoJane tape system (Instrumedics, Inc.).

The oim cell line was obtained from an immortalized primary culture of calvarial cells from an oim mouse.[10] The corresponding control cell line was the normal pre-osteoblast MC3T3 line (ATCC). Cells were grown to confluence for 3 weeks in a 6-well plate, fed with alpha minimal essential medium, β-glycerol phosphate , and ascorbic acid (25 μg/ml) to induce collagen secretion.

3 Results

3.1 *Collagen Secreted in Tissue Culture*

As an initial test of our hypothesis that SHG will be able to differentiate between normal and OI tissues, we began by comparing our results with that of a previously established model. Kobayashi et al. used electron microscopy to visualize secreted collagen by human fibroblasts in tissue culture and observed pronounced differences in normal and OI assembly.[12] Here we compare the morphology of collagen secreted from immortalized MC3T3 pre-osteoblasts (control) and oim calvarial cells in tissue culture. Cells were grown for 21 days and imaged in a fully hydrated environment. Representative SHG images collected in the forward direction of the secreted collagen matrix from normal and oim cells are shown in Fig. 1. The collagen fibrils secreted from MC3T3 cells in Fig. 1(a) forms a tightly woven mesh, where the empty spaces are the location of the cells, which are transparent in this modality. In strong contrast, the oim collagen network in Fig. 1(b), is characterized by longer, less densely packed fibrils. These results are in qualitative agreement with Kobayashi et al.[12] Based on this similarity, we suggest that SHG may be used as a diagnostic tool to detect abnormal collagen assembly following a skin biopsy. Additionally, SHG may provide insight into the collagen secretion process, as these experiments can be performed for the same cells over a course of days to weeks.

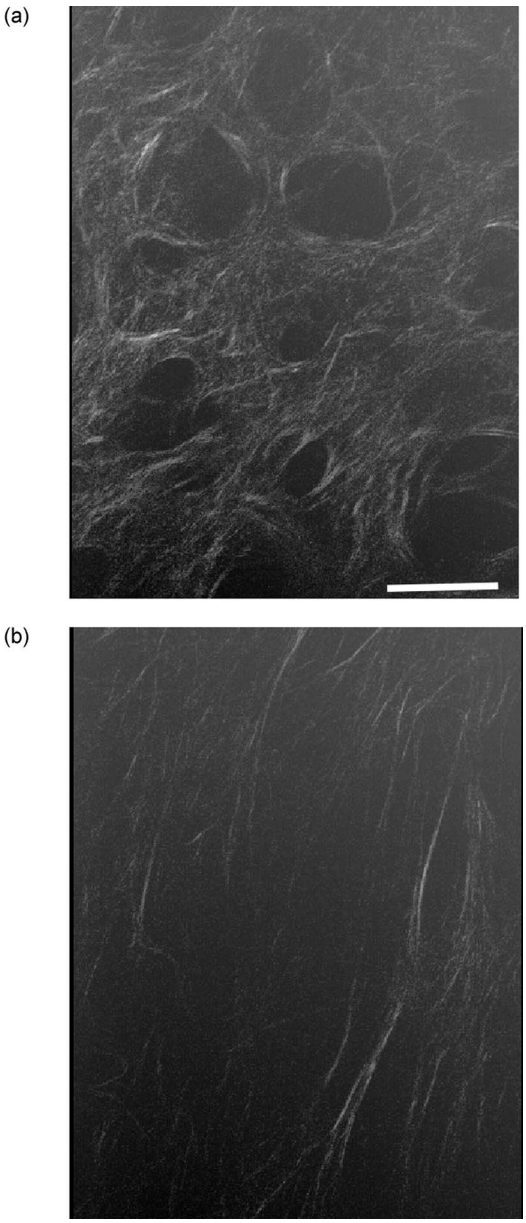

Fig. 1 Comparison of the collagen fibril morphology secreted from (a) MC3T3 pre-osteoblasts and (b) an oim calvarial derived line in tissue culture. The collagen fibrils are more well-packed for the wild type control. Scale bar =50 μm.

3.2 *Bone Morphology*

We examined whether the fibril morphology and organization of the collagen in WT and oim bone could be differentiated by SHG imaging. Figures 2(a) and 2(b) show representative images from cryosections of WT and oim, respectively, collected from the same region of the femur. While the collagen fibrils in bone lack the spatial regularity of tendon (shown later in Fig. 4), these images suggest that a more regular fibrillar structure is present in the WT. An initial assessment of the organization can be obtained by quantitatively comparing the integrated SHG intensities of the WT and oim. Integration of 10 image sets shows that the WT is characterized by $\sim$ twofold larger SHG intensity than the diseased state. As the SHG

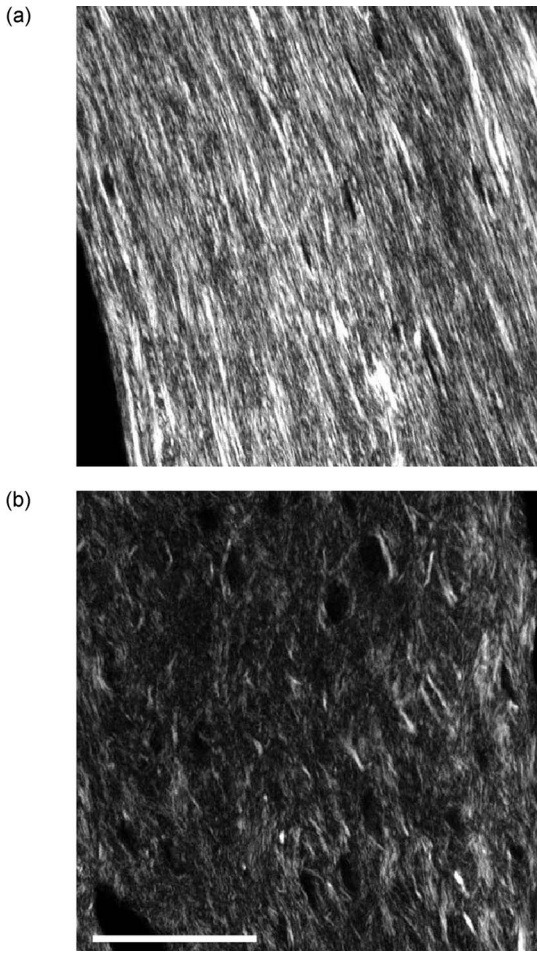

Fig. 2 Representative SHG images from cryosections of demineralized femur. Panels (a) and (b) are the wild type (WT) and oim, respectively. The WT has more regular fibrillar structure and stronger SHG intensity. Scale bar =50 μm.

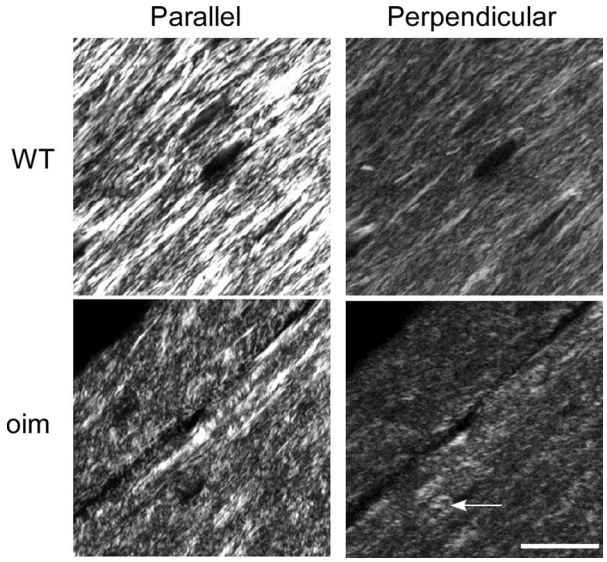

Fig. 3 SHG polarization anisotropy of WT (top row) and oim (bottom row) femur. The laser polarization was 45 deg with respect to the axis of the bone, and sequential images were obtained with a Glan polarizer parallel and perpendicular to the excitation. The oim has fibrillar components in both polarization states, indicating that the matrix is less organized than the WT. Scale bar=50 μm.

intensity is sensitive to both the local collagen concentration and the assembly, it is instructive to determine the cause of the intensity difference. While we cannot nondestructively measure the collagen concentration in these cryosections, later we show that this is similar for oim and WT skin. Thus, if we assume that the relative concentration of type I collagen is similar across tissue types, these results suggest that the decreased intensity from diseased bone arises from reduced organization. We note that these measurements were necessarily performed on fixed bone sections, as fresh bone undergoes a rapid autolysis, resulting in distortion of the tissue structure and consequently the optical properties. As shown in previous studies, such fixation does not significantly alter the fibrillar structure,[13] and this method is thus appropriate for comparison of tissues.

We can also make use of the SHG signal polarization anisotropy to further characterize the collagen assembly. As we have previously described, this measurement provides a determination of the order of the fibrils in each focal volume.[1,14] Here the laser polarization is fixed at the optimal angle (45 deg) relative to the long axis of the bone,[5] and two sequential SHG images are acquired with a polarizer oriented at 0 and 90 deg with respect to the input polarization. The results are shown in Fig. 3, where the top and bottom panels are the WT and oim, respectively. The WT images are dominated by parallel fibrils, where the parallel and perpendicular images are similar in morphology, suggesting that the signal comes primarily from highly aligned molecules in the assembly. In contrast, the organization is much more randomized for the oim bone, with no predominant fibril direction. This is further exemplified by the dissimilarity of the morphology in the parallel and perpendicular images, where many orthogonally oriented features appear for these two polarization states (see fibrils denoted by arrow). This suggests an underlying disorder in the collagen molecules that assemble into the fibrils. We have previously quantified such organization by calculating the resulting SHG anisotropy, β, by:

$$\beta = \frac{I_{par} - I_{orth}}{I_{par} + 2I_{orth}},$$

where I_{par} and I_{orth} are intensities of SHG signals polarized parallel and orthogonal to the polarization of excitation laser. This parameter can vary between -0.5 and 1, with a value of 0 representing the isotropic situation where I_{par} and I_{orth} are equal. Surprisingly, similar values of ~ 0.6 were obtained for both tissues. This arises because the fiber structure is fundamentally different. In the WT, the same fibrils appear in reduced intensity in the perpendicular direction, whereas in the oim, new features appear in the orthogonal direction. While strong morphological differences exist in these bone specimens, we thus conclude that the anisotropy parameter is not appropriate for analysis of this fibril topography. We will continue to work on new algorithms to quantify the polarization response for these complex morphologies. Yet we can confidently conclude that SHG imaging can reveal structural details not possible by standard histological microscopy.

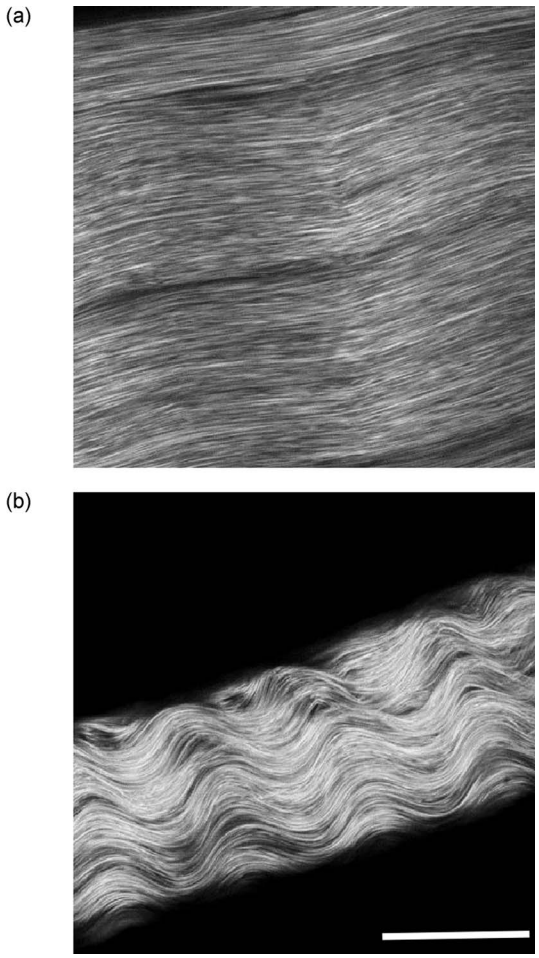

Fig. 4 Comparison of the crimping in (a) WT and (b) oim tendon SHG imaging. The oim has approximately a twofold increase in periodicity, suggesting that it has a decreased elastic modulus. Scale bar = 50 μm.

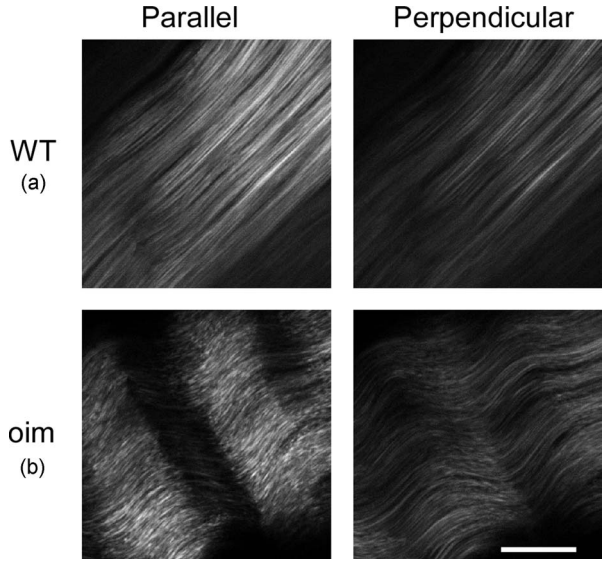

Fig. 5 Backward SHG polarization anisotropy of (a) WT and (b) oim tendon. The laser polarization was 45 deg with respect to the axis of the bone, and sequential images were obtained with a Glan polarizer parallel and perpendicular to the excitation. Smaller features are seen in the backward component of the oim tendon, resulting from a shorter coherence length and subsequent destructive interference of this coherent SHG component. These smaller fibrils are not observed in the forward channel (not shown). Scale bar = 20 μm.

3.3 *Tendon*

Previous scanning electron microscope (SEM) studies by McBride et al. showed that the fascicle cross sections of oim tendons were significantly smaller than those of the WT.[15] We further examine this issue to determine whether SHG can differentiate morphological and structural aspects at the smaller scale of assembly of fibrils and fibers in tendon. Forward-collected SHG images for the WT and oim tendon are shown in Figs. 4(a) and 4(b), respectively. We first measure the crimping, or the "waviness," in the tendons where the periodicity of the crimp is related to the material elastic modulus. The SHG images show that the characteristic frequency is much higher in the oim tissue. Average periodicities were 114 ± 15 μm ($n = 33$ fibrils) for the WT and 49 ± 6 μm ($n = 56$ fibrils) for the oim. We attribute the increased crimping in the oim to a decreased elastic modulus versus the WT. This result is consistent with decreased stiffness in oim bone and skin reported by other workers.[16,17]

Next we investigate whether the oim tendons are also comprised of smaller or less-packed fibrils. To this end, we exploit the directionality of the SHG emission. Backward-detected SHG can arise from either direct backward coherent emission or from multiple scattering of initially forward-directed photons. The first scenario is highly dependent upon the fibril diameters and packing. Fibrils in tissues much smaller than the SHG wavelength produce a symmetrical forward and backward emission distribution.[18,19] When the dipoles of adjacent molecules form aligned structures comparable to or larger than λ (in the axial dimension), the emission becomes highly forward directed. Due to the coherent nature of the SHG process, different fibril morphology can be observed in the forward and backward channels. Specifically, smaller features can be better visualized in the backward channel. This effect has been observed in collagen of tendon and cornea by Williams et al.[3] and Han et al.,[20] respectively, and more recently for fibrillar cellulose by Nadiarnykh et al.[14]

We compared the forward and backward signals with concurrent polarization anisotropy analysis to obtain the highest level of sensitivity to the supramolecular collagen structure. This approach yielded few discernible differences in the forward-collected geometry (not shown). In fact, calculation of the anisotropy parameter, β, results in a range of ~ 0.3 to 0.75 for both normal and diseased tissues. However, marked morphological differences are observed in the backward-collected geometry. Figures 5(a) and 5(b) show the parallel and perpendicular components of the backward-propagating SHG for the WT and oim, respectively. These images for the WT are highly similar. In contrast, the oim parallel channel displays smaller, segmented fibrils as well as longer, continuous fibrils. While differing in morphology, calculation of the anisotropy also results in a similar range of values to that in the forward channel.

To explain this appearance, we need to consider the fibril sizes. Our SEM analysis of the distribution of fibril sizes is

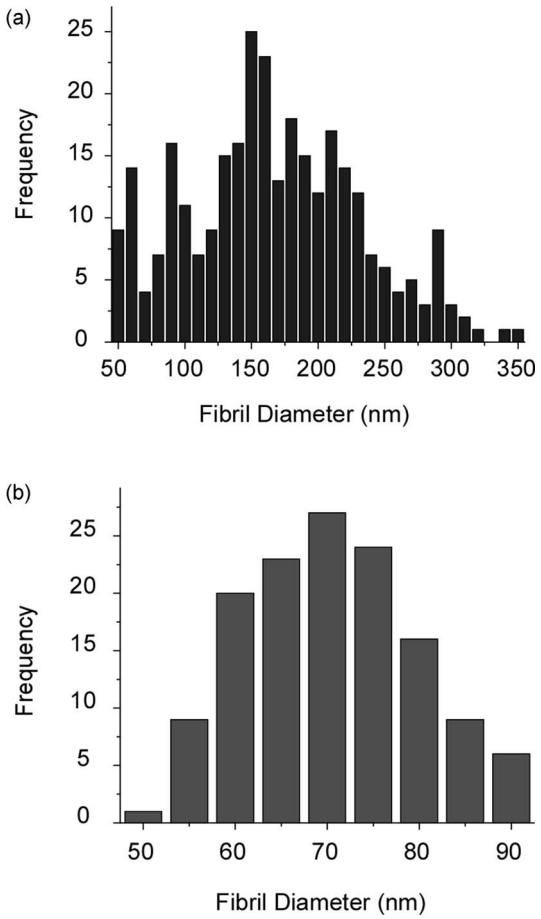

Fig. 6 Histogram of the fibril sizes as determined by SEM analysis of (a) WT and (b) oim tendon.

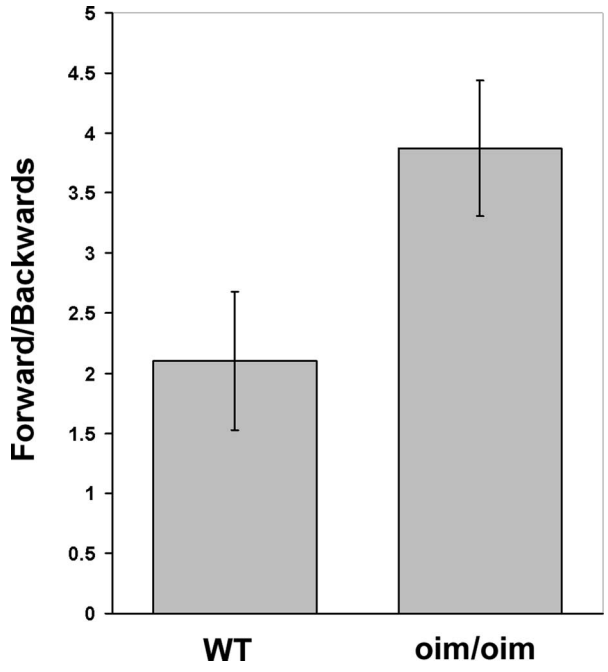

Fig. 7 Histogram of the measured F/B ratio of oim and WT tendon. The oim is more forward directed, indicative of a lower scattering coefficient and less dense matrix.

shown in the histogram in Fig. 6, where the most probable values for the oim (b) and WT (a) are ~70 and 160 nm, respectively. Elsewhere, we have provided a general treatment of the morphology observed in SHG images based on fibril size and packing, which predicts that the forward and backward channels will have different coherence lengths, where the visualization of segmented fibrils can arise from destructive interference in the latter.[19] Based on this work, we suggest that the contrast from these discontinuous-looking segmented fibrils is likely coherent (i.e., direct backward emission) arising from the smaller oim fibrils. We can then account for this segmented morphology primarily appearing in the parallel channel and the absence of these features in the perpendicular direction. We showed earlier that the forward SHG signal in these tendons is primarily polarized parallel to the laser electric field, and also that the forward and backward anisotropy in a fibrillar specimen were similar.[14] Thus, it is expected that the initial SHG backward emission here will have similar anisotropy. The backward-collected image is comprised of both coherent and incoherent multiple scattered components, and we suggest that the perpendicular image arises largely from multiple scattering of the forward signal, which does not display the segmented contrast. Upon scattering, the polarization of the signal will become randomized, and the signal will be captured in both backward polarization channels. We suggest that segmented appearing fibrils are not observed in the WT SHG images because of the larger diameter and concurrent longer coherence length. While both tissues are characterized by a similar range of anisotropies, the use of polarization analysis is essential to reveal the backward-coherent polarized emission on top of the depolarized multiple scattered component. Specifically, this uniquely shows the segmented appearance of the smaller fibrils in the oim tendon.

Unlike in bone, we cannot make a quantitative assessment of the relative SHG intensities in these samples because these fascicles are sufficiently thick (~50 to 100 μm) to support multiple-scattering events (the mean free path in such tissues is ~10 to 20 μm). As a result, the absolute intensity in each case will depend on the scattering coefficients at both the fundamental and SHG wavelengths, and due to differences in assembly, these parameters will be different in each tissue. However, we can exploit the directionality of the SHG signal propagation as a means to probe the density of the fibrillar packing. The forward-to-backward ratio (F/B) that arises from multiple scattering of the forward signal will depend on the magnitude[14] of the reduced scattering coefficient μ_s'. We have not yet been able to measure these coefficients in mouse tendon but have measured the F/B intensities in WT and oim tendon. A histogram of the results obtained by integrated z projection of the SHG intensity is shown in Fig. 7, where the mean F/B values for the normal and diseased mice are 2.1 ± 0.6 and 3.5 ± 0.6, respectively. The increased scattering in the WT (i.e., lower F/B) is also consistent with the higher degree of similarity in the polarized SHG images in Fig. 5(a), where both channels contained a significant multiple-scattered component. Conversely, the more forward directed signal for the oim is consistent with a less dense matrix, as the mean free path will be longer and there is lower probability for

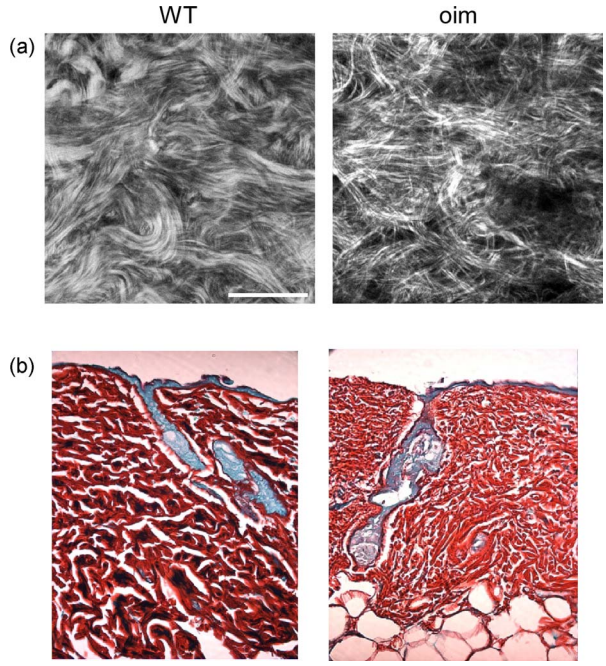

Fig. 8 Morphology of WT and oim skin determined by (a) SHG and (b) histological staining with Sirius Red and Fast Green FCF. Both contrasts show denser packing of the collagen fibrils for the WT relative to the oim. Scale bar=50 μm. (Color online only.)

multiple collisions. We therefore suggest that this finding is consistent with sparser packing of fibrils in the matrix and the mechanical properties *in vivo*, and that this approach of measuring propagation could be used as a diagnostic tool.

3.4 *Skin*

Our long-term goal is to develop SHG imaging as a clinical diagnostic tool. For both *ex vivo* and *in vivo* imaging, skin is the most accessible tissue, and to this end, we examine whether SHG can quantitatively differentiate WT and oim skin. Representative images are shown in Figs. 8(a) and 8(b), respectively, where these were taken at depths into the dermis of ~20 microns (plus ~10 μm of the epidermis). Based on our SEM analysis, the average fibril sizes in the oim and WT skin are ~70 and 100 nm, respectively, and cannot be resolved in the SHG microscope. However, on inspection, these images suggest that the fibrils are less ordered for the diseased skin. As the SHG contrast depends on the square of the concentration of the sources as well as their molecular organization, we need to determine the contributions of these effects. To this end, the tissues were stained with Sirius Red and Fast Green FCF to assess the collagen and total protein content, respectively. These histological sections are shown in Figs. 8(c) and 8(d), respectively. We first note that the Sirius Red staining appears more highly packed in the dermal assembly for the WT and is consistent with the tighter packing seen in the SHG image. Quantitative measurements of the extracted Sirius Red showed that the collagen content in the oim was 85% that of the WT. Given this similarity, we ascribe the higher degree of SHG contrast difference between WT and oim skin to reduced collagen organization in the diseased tissue.

We must be able to extract quantitative differences to apply the method as a disease diagnostic. The complex morphology of skin does not lend itself to polarization anisotropy. Indeed, attempts to determine β led to a random distribution, even when performed over several ranges of size scales in the images. However, we can readily perform relative assessments of the organization and packing by measurement of the F/B as described earlier for tendon as a means of comparing the scattering properties. These measurements obtained by integrated average z projections of 3-D image stacks show F/B values of 2.6 ± 0.3 and 1.6 ± 0.2 for the oim and WT, respectively. These values follow the same trends observed in tendon, being indicative of a smaller reduced scattering coefficient, and similarly indicating that the oim tissue is less organized than the WT. This result suggests that SHG imaging of skin can be used as a quantitative assessment of this disorder.

4 Discussion

Many approaches have been employed to understand the structural differences in the collagen fiber organization in normal and OI tissues. The triple helical structure and intramolecular organization of collagen fibrils has been the subject of the number of x-ray diffraction and NMR studies. X-ray diffraction analysis of collagen-like peptides shows the destabilizing effect of a glycine point mutation. Similar studies using biochemical methods[21] or NMR and circular dichroism (CD) lead to a similar conclusion.[22–24] At the intramolecular level, x-ray diffraction has shown small fibers with less well defined lateral growth and more fiber disorganization in tissue obtained from OI subjects.[15] Collectively, these structural studies indicate a decreased level of organization in OI tissue, which ultimately leads to decreased bone strength. We extend these ideas to 3-D imaging microscopy of *ex vivo* tissues. Our rationale was to exploit the exquisite sensitivity of SHG to supramolecular assembly to differentiate between the respective fibrillar structures in normal and diseased tissues.

As a first step, we have demonstrated that by employing several different metrics, SHG imaging can indeed be applied to the oim mouse model. The constraint that SHG requires a noncentrosymmetric environment to generate contrast yields the ability to probe the fibrillar organization and thus provides greater structural information than possible by fluorescence or other optical microscopies. For example, tendon crimping has been traditionally studied by polarization microscopy of cryosections.[25] However, SHG reveals greater contrast of the fibrils in the fascicles than is possible by probing only the birefringence. The crimping had been considered as a planar effect, but through indirect evidence, recent work suggests that the fibrils formed helical structures.[26] Inspection of the SHG images in Fig. 4 reveals this geometry directly. This method also provides greater information content than the historical gold standard of histology. For example, 3-D images can be obtained without the use of slicing, fixation, and staining. Furthermore, as demonstrated in Fig. 7, SHG provides higher-resolution, higher-contrast visualization of the collagen assembly than is possible by histological staining. In sum, this approach has significant advantages over conventional imaging methods because SHG directly visualizes the collagen supramolecular structure without relying on inferences from exogenous labels.

Additional richness lies in the coherent nature of the SHG contrast mechanism. We showed that smaller oim tendon fibrils were visible exclusively in the backward collection geometry. Noncoherent contrast modalities including fluorescence and polarization microscopy cannot reveal these details. We further showed that SHG could differentiate WT and oim tissues based on the directionality of the measured signal, because this direction arises in part from the underlying reduced scattering coefficient, μ_s'. This measurement is enabled both by the ability to optically section through the tissues and by the coherent origin of SHG emission. This approach affords quantitative comparisons of the structural organization based on differences in photon migration behavior. In tissues such as skin, where the complex fibrillar structure makes numerical morphological assessments and pattern recognition difficult, quantifying SHG scatter through F/B and polarization anisotropy measurements produces a probe of collagen density and assembly.

While the current work shows the ability of SHG to differentiate normal and diseased states in the oim mouse model, we suggest that this work provides justification for pursuit of the SHG modality as a future clinical diagnostic tool for human OI. Historically, bone biopsies have been the standard of care for assessment of disease severity or efficacy of treatment. However, this is a highly invasive procedure. Ultimately, we hope to use SHG imaging skin *in vivo* in the backward collection direction as a clinical probe of human OI. However, even if biopsies are required, this is a less-invasive test for skin than bone. Our observation that SHG can optically discriminate normal and diseased oim skin lays the foundation for pursuing this approach.

5 Conclusions

Through these studies, we have used quantitative SHG imaging to derive several metrics for comparison of the tissue organization in WI and oim bone, tendon, and skin. These findings are enabled by the sensitivity of the approach to the supramolecular assembly. Through intensity comparisons, morphological comparisons, polarization analysis, and SHG signal propagation, we showed that statistically different results are obtained for the normal and diseased state. All these optical signatures are consistent with the collagen matrix in the oim tissues being more disordered, where these results are consistent with the known weaker mechanical properties of the oim mouse. We suggest that the current approach will complement the existing ultrastructural data in that imaging could be performed either *in vivo* or immediately *ex vivo* in intact tissues and be eventually used as a diagnostic tissue or measure of treatment efficacy. Additionally, the SHG metrics described could be applied to other connective tissue disorders that are characterized by abnormal collagen assembly.

Acknowledgments

We thank Prof. David Rowe for suggesting this work and Prof. Doug Adams for helpful scientific discussions. PJC and WAM gratefully acknowledge support under NIH EB-01842 and IK gratefully acknowledges support from the Osteogenesis Imperfecta Foundation.

References

1. P. J. Campagnola, A. C. Millard, M. Terasaki, P. E. Hoppe, C. J. Malone, and W. A. Mohler, "3-dimensional high-resolution second harmonic generation imaging of endogenous structural proteins in biological tissues," *Biophys. J.* **82**, 493–508 (2002).
2. A. Zoumi, A. Yeh, and B. J. Tromberg, "Imaging cells and extracellular matrix *in vivo* by using second-harmonic generation and two-photon excited fluorescence," *Proc. Natl. Acad. Sci. U.S.A.* **99**, 11014–11019 (2002).
3. R. M. Williams, W. R. Zipfel, and W. W. Webb, "Interpreting second-harmonic generation images of collagen I fibrils," *Biophys. J.* **88**, 1377–1386 (2005).
4. S.-P Tai, T.-H Tsai, W.-J Lee, D.-B Shieh, Y.-H Liao, H.-Y Huang, K. Zhang, H.-L. Liu, and C.-K. Sun, "Optical biopsy of fixed human skin with backward-collected optical harmonics signals," *Opt. Express* **13**, 8231–8242 (2005).
5. S. V. Plotnikov, A. C. Millard, P. J. Campagnola, and W. A. Mohler, "Characterization of the myosin-based source for second-harmonic generation from muscle sarcomeres," *Biophys. J.* **90**, 693–703 (2006).
6. F. Vanzi, M. Capitanio, L. Sacconi, C. Stringari, R. Cicchi, M. Canepari, M. Maffei, N. Piroddi, C. Poggesi, V. Nucciotti, M. Linari, G. Piazzesi, C. Tesi, R. Antolini, V. Lombardi, R. Bottinelli, and F. S. Pavone, "New techniques in linear and non-linear laser optics in muscle research," *J. Muscle Res. Cell Motil.* **27**, 469–479 (2006).
7. W. R. Zipfel, R. M. Williams, R. Christie, A. Y. Nikitin, B. T. Hyman, and W. W. Webb, "Live tissue intrinsic emission microscopy using multiphoton-excited native fluorescence and second harmonic generation," *Proc. Natl. Acad. Sci. U.S.A.* **100**, 7075–7080 (2003).
8. E. Brown, T. McKee, E. diTomaso, A. Pluen, B. Seed, Y. Boucher, and R. K. Jain, "Dynamic imaging of collagen and its modulation in tumors *in vivo* using second-harmonic generation," *Nat. Med.* **9**, 796–800 (2003).
9. S. J. Lin, S. H. Jee, C. J. Kuo, R. J. Wu, W. C. Lin, J. S. Chen, Y. H. Liao, C. J. Hsu, T. F. Tsai, Y. F. Chen, and C. Y. Dong, "Discrimination of basal cell carcinoma from normal dermal stroma by quantitative multiphoton imaging," *Opt. Lett.* **31**, 2756–2758 (2006).
10. S. D. Chipman, H. O. Sweet, D. J. McBride Jr., M. T. Davisson, S. C. Marks Jr., A. R. Shuldiner, R. J. Wenstrup, D. W. Rowe, and J. R. Shapiro, "Defective pro alpha 2(I) collagen synthesis in a recessive mutation in mice: a model of human osteogenesis imperfecta," *Proc. Natl. Acad. Sci. U.S.A.* **90**, 1701–1705 (1993).
11. J. Saban and D. King, "PCR genotyping of oim mutant mice," *BioTechniques* **21**, 190–192 (1996).
12. K. Kobayashi, R. Hata, S. Nagai, J. Niwa, and T. Hoshino, "Direct visualization of affected collagen molecules synthesized by cultured fibroblasts from an osteogenesis imperfecta patient," *Biochem. Biophys. Res. Commun.* **172**, 217–222 (1990).
13. K. M. Meek, "The use of glutaraldehyde and tannic acid to preserve reconstituted collagen for electron microscopy," *Histochemistry* **73**, 115–120 (1981).
14. O. Nadiarnykh, R. B. LaComb, P. J. Campagnola, and W. A. Mohler, "Coherent and incoherent SHG in fibrillar cellulose matrices," *Opt. Express* **15**, 3348–3360 (2007).
15. D. J. McBride Jr., V. Choe, J. R. Shapiro, and B. Brodsky, "Altered collagen structure in mouse tail tendon lacking the alpha 2(I) chain," *J. Mol. Biol.* **270**, 275–284 (1997).
16. N. P. Camacho, L. Hou, T. R. Toledano, W. A. Ilg, C. F. Brayton, C. L. Raggio, L. Root, and A. L. Boskey, "The material basis for reduced mechanical properties in oim mice bones," *J. Bone Miner. Res.* **14**, 264–272 (1999).
17. B. Hansen and G. B. Jemec, "The mechanical properties of skin in osteogenesis imperfecta," *Arch. Dermatol.* **138**, 909–911 (2002).
18. J.-X Cheng, A. Volkmer, L. D. Book, and X. S. Xie, "An epi-detected coherent anti-Stokes Raman scattering (E-CARS) microscope with high spectral resolution and high sensitivity," *J. Phys. Chem. B* **105**, 1277–1280 (2001).
19. R. Lacomb, O. Nadiarnykh, S. S. Townsend, and P. J. Campagnola, "Phase matching considerations in second harmonic generation from tissues: effects on emission directionality, conversion efficiency, and observed morphology," submitted to *Opt. Commun.* (in press).
20. M. Han, G. Giese, and J. F. Bille, "Second harmonic generation imaging of collagen fibrils in cornea and sclera," *Opt. Express* **13**, 5791–5797 (2005).

21. K. Beck, V. C. Chan, N. Shenoy, A. Kirkpatrick, J. A. Ramshaw, and B. Brodsky, "Destabilization of osteogenesis imperfecta collagen-like model peptides correlates with the identity of the residue replacing glycine," *Proc. Natl. Acad. Sci. U.S.A.* **97**, 4273–4278 (2000).
22. X. Liu, S. Kim, Q. H. Dai, B. Brodsky, and J. Baum, "Nuclear magnetic resonance shows asymmetric loss of triple helix in peptides modeling a collagen mutation in brittle bone disease," *Biochemistry* **37**, 15528–15533 (1998).
23. J. Baum and B. Brodsky, "Folding of peptide models of collagen and misfolding in disease," *Curr. Opin. Struct. Biol.* **9**, 122–128 (1999).
24. G. Melacini, A. M. Bonvin, M. Goodman, R. Boelens, and R. Kaptein, "Hydration dynamics of the collagen triple helix by NMR," *J. Mol. Biol.* **300**, 1041–1049 (2000).
25. M. Franchi, M. Fini, M. Quaranta, V. De Pasquale, M. Raspanti, G. Giavaresi, V. Ottani, and A. Ruggeri, "Crimp morphology in relaxed and stretched rat Achilles tendon," *J. Anat.* **210**, 1–7 (2007).
26. B. de Campos Vidal, "Image analysis of tendon helical superstructure using interference and polarized light microscopy," *Micron* **34**, 423–432 (2003).